Effect of Thermal Ageing of Pd/Al_2O_3 Catalyst on the Selectivity of NH_3 Formation

YAO Li-peng[1], WANG Cheng-xiong[1, 2], TAN Jian-wei[3], REN De-zhi[1], ZHENG Ting-ting[2], ZHAO Yun-kun[1, 2 *]

(1. State Key Laboratory of Advanced Technologies for Comprehensive Utilization of Platinum Metals, Kunming Institute of Precious Metals, Kunming 650106, China;
2. State-Local Joint Engineering Laboratory of Precious Metal Catalytic Technology and Application, Kunming Sino-platinum Metals Catalysts Co. Ltd., Kunming 650106, China;
3. School of Mechanical Engineering, Beijing Institute of Technology, Beijing 100081, China)

Abstract: The effect of thermal aging on the selectivity of NH_3 products in three-way catalytic reaction was studied. Steady-state experiments were carried out in dilute/rich circulating flow. X-ray diffraction (XRD), BET specific surface area, X-ray photoelectron spectroscopy (XPS), Raman spectroscopy (Raman) and transmission electron microscopy (TEM) were used to characterize the physicochemical properties of the catalysts. The results showed that high temperature aging led to a decrease in the dispersion of palladium, an increase in particle size and a decrease in the relative proportion of the Pd^{2+} active species. These microstructural changes contribute to the reduction of the three-way activity of catalysts, resulting in the increase in ammonia selectivity. Thermal ageing induces a significant increase in active palladium particles on the catalyst surface, and larger particles promotes NO to dissociate to form active nitrogen species, which in turn react with hydrogen to form NH_3.

Key words: Pd/Al_2O_3 catalyst; thermal ageing; NH_3 formation; three-way catalytic reactions(TWC); Pd particle

CLC number: O643.3 **Document code:** A **Article ID:** 1004-0676(2020)01-0001-09

热老化对 Pd/Al_2O_3 选择性催化 NH_3 反应性能的影响

姚丽鹏[1]，王成雄[1,2]，谭建伟[3]，任德志[1]，郑婷婷[2]，赵云昆[1,2 *]

(1. 昆明贵金属研究所 稀贵金属综合利用国家重点实验室，昆明 650106；
2. 昆明贵研催化剂有限责任公司 贵金属催化技术与应用国家地方联合工程实验室，昆明 650106；
3. 北京理工大学 机械与车辆学院，北京 100081)

摘 要：研究了在三效催化反应过程中热老化对 Pd/Al_2O_3 选择性催化 NH_3 反应性能的影响。在稀/富循环流中进行稳态实验，采用 X 射线衍射(XRD)、BET 比表面积、X 射线光电子能谱(XPS)、拉曼光谱(Raman)和透射电镜(TEM)对催化剂的物理化学性质进行表征。结果表明，高温热老化导致活性金属钯的分散度降低、颗粒尺寸增大、Pd^{2+}活性物种的相对比例下降，这些微结构变化促使催化剂的三效活性降低、氨选择性增加。热老化诱导催化剂表面活性钯颗粒明显增大，较大的钯颗粒有助于 NO 解离生成活性氮物种，进而与氢反应生成 NH_3。

关键词：Pd/Al_2O_3 催化剂；热老化；NH_3 生成；三效催化反应(TWC)；Pd 颗粒

收稿日期：2019-05-16
基金项目：国家自然科学基金(51676017, 21862010)、云南省科技人才和平台计划项目(2018IC091)、云南省重大科技专项(2018ZE017)
第一作者：姚丽鹏，男，硕士研究生，研究方向：贵金属催化剂。E-mail：ylpppp@163.com
*通讯作者：赵云昆，男，研究员，研究方向：汽车尾气后处理技术。E-mail：yk.zhao@spmcatalyst.com

Automotive exhaust gases comprising of carbon monoxide (CO), nitrogen oxides (NO_x), and unburned hydrocarbons (HCs) contribute to global warming, ozone layer depletion, acid rain and environmental toxicity[1-2]. Three-way catalysts (TWCs), up to now, are the most satisfactory and efficient solution to diminish CO, NO_x, and HCs emissions from gasoline engines. The use of Pd as the only active metal component in TWC has received considerable attention on the basis of economical aspects (the high cost and scarcity of Rh). Pd-only three-way catalyst is used in the automotive industry to reduce harmful emissions that contain CO, NO_x and HCs[3-5], but leading to an increase in undesired NH_3 and N_2O emissions [6-8]. Durbin et al.[9] reported that emission rates of NH_3 for a fleet consisted of light-duty trucks and light-duty passenger vehicles averaged 34 mg/km with a range of 2.5 to 110 mg/km, although the fleet of vehicles was certified at the ULEV standard for California. Heeb et al.[10] found that the average NH_3 emission rates were 16±12 mg/km and 10±7 mg/km for gasoline-fueled Euro-3- and Euro-4-passenger cars, respectively. NH_3 acts as a precursor of NH_4^+ ion to form secondary inorganic aerosols, which reacts with nitrogen to form particulate matter (NH_4NO_3)[11-12].

Although the mechanisms of NH_3 formation during three-way catalytic reactions are complex, there are still some related mechanisms reported. For example, Mejía-Centeno et al.[5] suggested that hydrogen produced in the steam reforming (SR) and water gas-shift (WGS) reactions is a major contributor to NH_3 formation through the overall reaction of $2NO+2CO+3H_2\rightarrow 2NH_3+2CO_2$ or $NO+5H_2\rightarrow 2NH_3+2H_2O$. In addition, Adams et al.[13] found that $Pd/Ce/Al_2O_3$ catalyst showed a higher selectivity of NH_3 formation, compared to that of Pd/Al_2O_3 catalyst, owing to the promotional effects of ceria on SR and WGS reactions. As reported by Durbin et al.[14], bench rapid ageing lead to an increase in the amount of NH_3 emissions, according to the vehicle testing results. Our group[11] also proposed the mechanisms of hydroxyl-mediated NH_3 formation on the $Rh-CeO_2$ catalyst surface. In the presence of water, water-induced hydroxylation could promote NH_3 formation, whereas the competitive adsorption of H_2O and NO on the same sites would inhibit the reactivity of NO reduction by NH_3, leading to an increase in NH_3 emission.

In this study, we used Pd-only catalyst supported by γ-Al_2O_3. This is because the decreased oxygen storage capacity (OSC) of TWC induced by ageing will result in activity loss of NH_3 oxidation under rich conditions[12]. In order to study the influence of OSC-free catalyst structure changes caused by ageing on the selectivity of ammonia, the generation and structure characterization of Pd/Al_2O_3 catalyst after ageing in the three-way catalytic reaction process were carried out, providing a basis for NH_3 emission control.

1 Experimental

1.1 Catalyst preparation

Pd/Al_2O_3 (1.0%, by weight) catalyst was prepared on incipient wetness impregnation method. $Pd(NO_3)_2$ (Kunming Institute of Precious Metals 24%) and γ-Al_2O_3 (Aladdin Industrial Corporation, 20 nm) were used as the starting materials. Al_2O_3 powder was dispersed in 450 mL demonized water. Then $Pd(NO_3)_2$ solution was added under continuous agitation. Dipping mixture and stirring at room temperature for 5 h, then drying overnight at 140°C. After calcination at 600°C in static air for 5 h, the fresh catalyst was obtained, followed by aged at 800°C and 1000°C in static air for 5 h, respectively.

1.2 Catalyst characterization

The specific surface areas of samples were measured using the N_2 adsorption at -196°C by the Brunauer-Emmett-Teller(BET) method on an automatic surface analyzer (Quantachrome Nova-2200e). Prior to the measurements, the samples were degassed under vacuum at 200°C for 2 h.

The Pd dispersion on Pd-containing catalyst was determined by CO chemisorption at 100°C in a ChemBET Pulsar. Prior to each CO measurement, the catalyst was heated to 450°C in Argon for 60 min. After cooling to 100°C, the CO adsorption experiment was performed using CO pulse method. A ratio of CO/Pd was used for the amount calculation of Pd atoms on the surface. Actual content of Pd was analyzed on PerkinElmer Optima 8000 ICP-OES instrument. The total Pd atoms were calculated from actual content of Pd in catalyst.

The X-ray diffraction (XRD) analysis of sample was performed on an X'Pert Pro diffractmeter (Japan) using Cu Kα radiation. The operating voltage is 36 kV. And the working current is 30 mA. The data for step scanning XRD were recorded at 0.02^o intervals in the range $10^o \leqslant 2\theta \leqslant 80^o$.

The XPS experiments were performed on a spectrometer (Thermo Fisher Scientific) equipped with a monochromatic Al Kα X-rays under ultra-high vacuum (2×10^{-7} mba). Sample charging during the measurement was compensated by an electron flood gun. The binding energy was calculated internally by the carbon deposit C1s binding energy (BE) at 284.8 eV.

Transmission electron microscopy (TEM) images were taken on a JEM-2100 transmission electron microscope with an accelerating voltage of 200 kV.

Raman measurements were carried out on a Renishaw Raman 2000 system spectrometer with a spectral resolution of 1 cm^{-1}. The acquisition was run for a 10 s exposure time for collection of a single spectrum with a 532.5 nm laser excitation source after 30 min of stabilization at each temperature step. Before the measurement, the Raman tool was calibrated with a crystalline Si wafer with the characteristic peak observed at 519.6 cm^{-1}. A low laser power of 0.1 mW (power density of 8 μw/μm^2) on the sample was used in all measurements to avoid laser heating without using any neutral density filters. The experimental spectra were analyzed with theoretical models that include phonon interactions and thermal expansion effects and possible phonon decay channels identified.

Temperature-programmed reduction of the samples in hydrogen was carried out in a flow installation with a thermal conductivity detector (TCD) using the powder catalyst fraction. Prior to the TPR experiments, the samples were treated in an Ar steam for 1 h at 350°C and cooled down to 10°C in this condition. The mass of the samples was 100 mg. TPR was carried out in a 75 mL/min flow of the reducing mixture containing 10% H_2 in Ar. The samples were heated in this flow from 10°C to 800°C with 10°C/min of heating rate. The consumption of H_2 was detected by TCD.

1.3 Catalytic activity measurement

The three-way catalytic reactions on Pd/Al_2O_3 catalyst were employed in a continuous flow fixed-bed micro-reactor. 500 mg catalysts with an average diameter 40~60 mesh were placed in a stainless-steel tube with an inner diameter of 5 mm. The catalysts were activated at 550°C in 21% O_2/N_2 stream for 30 min. Steady-state experiments were conducted in a lean/rich cycling (1.67×10^{-2} Hz) stream with total flow rate of 500 mL/min and the space velocity (Sv = 60000 $mL\cdot g^{-1}\cdot h^{-1}$) at every 25°C from 175°C to 550°C. Rich condition: 0.1%CO, 0.05%NO, 0.1%C_3H_6, 8%CO_2, 5%H_2O, 0.1%O_2, N_2 balance. Lean condition: 0.1%CO, 0.05%NO, 0.1%C_3H_6, 8%CO_2, 5%H_2O, 0.86%O_2, N_2 balance. The composition of the effluent gas was analyzed online using a 2030DBG2EZKS13T MultiGas FTIR Analyzer. The conversion rate of CO, α(CO, %) was calculated by following Eq. (1):

$$\alpha(\mathrm{CO},\ \%) = \{[\mathrm{CO}]_{in}-[\mathrm{CO}]_{out}\}/[\mathrm{CO}]_{in}\times100\% \qquad (1)$$

Where $[\mathrm{CO}]_{in}$ and $[\mathrm{CO}]_{out}$ represent the concentration of the injected and effluent CO gas, respectively. The values of NO and C_3H_6 conversion rate were calculated by the same method. The selectivity of NH_3 and N_2O, S(N_2O, %), S(NH_3, %), were calculated by the Eqs. (2)~(3) based on the concentration of NH_3 and N_2O products, respectively[15].

$$S(\mathrm{N_2O},\ \%)=\{[\mathrm{NO}]_{in}-[\mathrm{NO}]_{out}\}/2[\mathrm{N_2O}]_{out}\times100\% \qquad (2)$$

$$S(\mathrm{NH_3},\ \%)=\{[\mathrm{NO}]_{in}-[\mathrm{NO}]_{out}\}/[\mathrm{NH_3}]_{out}\times100\% \qquad (3)$$

$$S(\mathrm{N_2},\ \%)=100-S_{\mathrm{N_2O}}-S_{\mathrm{NH_3}} \qquad (4)$$

2 Results and discussion

2.1 XRD and BET surface area

Fig.1 shows XRD patterns of different catalysts. The XRD pattern of the fresh catalyst exhibits the characteristic peaks of γ-Al_2O_3 and there is no obvious diffraction peaks of PdO and Pd. However, the diffraction peak of PdO becomes sharpened clearly after ageing at 800°C, which indicates that the size of

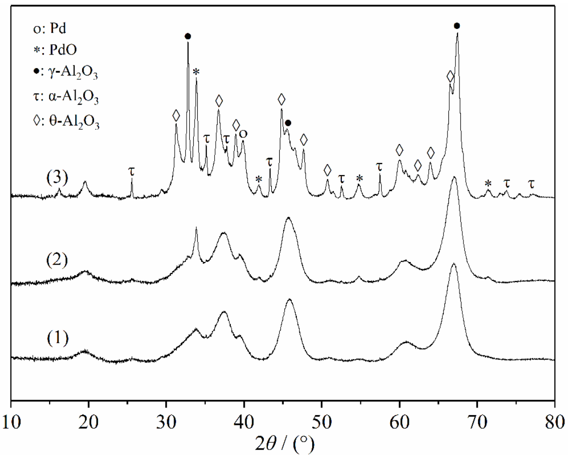

(1). Fresh(新制); (2). 800°C-aged (800°C 老化);

(3). 1000°C-aged(1000°C 老化)

Fig.1 XRD patterns of various catalysts

图 1 不同催化剂的 XRD 图谱

Pd particles increased after ageing[16]. Increasing ageing temperature to 1000°C results in a slight decomposition of PdO to metallic Pd, evidence in line at $2\theta = 40.1°$ [17-19], and a sharper diffraction peak of PdO than that of 800°C-aged catalyst, which illustrates occurrence of Pd particles with increased size . And it shows a poor Al_2O_3 phase transformation from γ-Al_2O_3 to θ-Al_2O_3 according to the XRD pattern of the 800°C-aged samples. However, the clear diffraction peaks of α-Al_2O_3 and θ-Al_2O_3 phase can be seen after ageing at 1000°C.

Tab.1 Textual properties obtained from N_2 adsorption and Pd dispersion of catalysts

表 1 不同催化剂的 N_2 吸附和 Pd 分散度性质

Sample	Pd/%^{a}	S_{BET}/ (m^2/g)	Dispersion/ %^{b}	Dp (Pd^0)/nm^c
Fresh	0.99	187.7	37.4	3.0
800°C-aged	1.01	157.1	28.0	4.0
1000°C-aged	1.04	112.7	6.1	18.4

^{a} Detected by ICP-OES analysis;

^{b} Calculated by assuming that CO adsorbs stoichiometrically to surface Pd atoms;

^{c} Based on formula $D_p = 1.12/D$ (nm), where D represents Pd dispersion.

The values of BET surface area (S_{BET}) of the samples are displayed in Tab.1. As listed in Tab.1, the surface area of fresh catalyst is 187.7 m^2/g, while the catalysts aged at 800°C and 1000°C have lower surface area, and their surface area are 157.1 m^2/g and 112.7 m^2/g, respectively. The decrease in specific surface area induced by high ageing temperature is related to alumina transformation[20]. The crystal structure of γ-Al_2O_3 will change at higher ageing temperature. The inner reticular structure is destroyed, resulting in the internal voids collapse or close, an increase in the crystal particles, and smaller specific surface area. At this time, the γ-Al_2O_3 will produce phase trans- formation, form θ-Al_2O_3 or α-Al_2O_3. This result is consistent with XRD patterns. The Pd metals are dispersed on the surface of γ-Al_2O_3 and γ-Al_2O_3 is converted into θ-Al_2O_3 or α-Al_2O_3 at high temperature, so most of the catalysts are covered by a thin Al_2O_3 layer in the crystal structure and can not be contacted and utilized by gas, and the catalysts are basically deactivated.

2.2 XPS and Raman

XPS was used to determine the chemical states of the active Pd species in catalysts. Fig.2 shows Pd 3d XPS spectra. The peaks centered at 341.0 eV, 335.9 eV, 342.2 eV and 337.0 eV in Pd 3d XPS spectra of catalyst samples can be assigned to $Pd^0 3d_{3/2}$, $Pd^0 3d_{5/2}$, $Pd^{2+} 3d_{3/2}$ and $Pd^{2+} 3d_{5/2}$, respectively[21-23].

The values of surface $Pd^{2+}/(Pd^0+Pd^{2+})$ in different catalysts were obtained from the integral area of the spectral components in $Pd^0 3d_{5/2}$ and $Pd^{2+} 3d_{5/2}$ and given in Tab.2. A slight decrease in surface $Pd^{2+}/(Pd^0+Pd^{2+})$ of 1000°C-aged catalyst indicates the formation of metallic Pd, which is well agreement with XRD results.

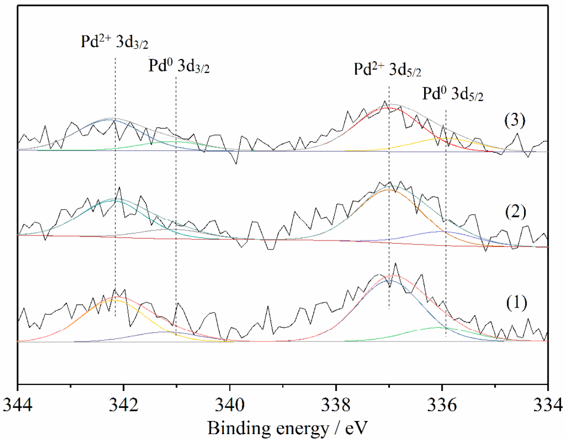

(1). Fresh(新制); (2). 800°C-aged (800°C 老化); (3). 1000°C-aged(1000°C 老化)

Fig.2 XPS spectra of various samples

图 2 不同催化剂的 XPS 图谱

Tab.2 XPS data of various samples

表 2 不同样品的 XPS 数据

Sample		Pd $3d_{5/2}$			Pd $3d_{3/2}$			$Pd^{2+}/(Pd^{2+}+Pd^0)^a$ / %
		BE	Aera	FWHM	BE	Aera	FWHM	
Fresh	Pd^0	336.06	260	1.50	341.21	180	1.50	80.8
	Pd^{2+}	336.99	1098	1.51	342.19	760	1.49	
800°C-aged	Pd^0	335.97	250	1.50	341.08	173	1.50	79.4
	Pd^{2+}	336.98	966	1.50	342.20	669	1.49	
1000°C-aged	Pd^0	335.95	245	1.48	341.10	170	1.50	76.5
	Pd^{2+}	337.02	799	1.50	342.28	553	1.52	

^{a} Obtained from the integral area of the spectral components in Pd^0 $3d_{5/2}$ and Pd^{2+} $3d_{5/2}$.

Structural information of the catalysts is also measured by Raman. The Raman spectra are given in Fig.3. All samples shows a peak centered at 645 cm^{-1}, illustrating the existence of PdO phase[24-26]. Moreover, the additional weak peaks at about 277, 339 and 567 cm^{-1} are also derived from the PdO phase[26]. The result is well consistent with the results of XRD and XPS.

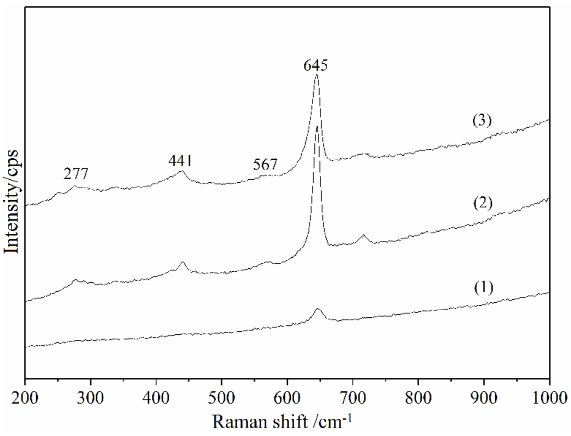

(1). Fresh(新制); (2). 800°C-aged (800°C 老化);

(3). 1000°C-aged(1000°C 老化)

Fig.3 Raman spectra of the different samples

图 3 不同催化剂的 Raman 图谱

2.3 TEM and Pd dispersion

Fig.4 shows TEM images of catalysts. The size of Pd particle in fresh catalyst is with average dimensions of 3 nm. As the ageing temperature increased to 800°C, the Pd particle size slightly increased, reaching ~4 nm. It can be seen that the size of Pd particle in 1000°C-aged sample is about 18 nm, indicating significant sintering and agglomeration of Pd particle induced by ageing at 1000°C. As displayed in Tab.1, the Pd dispersion of fresh and 800°C-aged samples is 37.4% and 28.0%, respectively, and the corresponding Pd particle sizes are 3.0 nm and 4.0 nm. While the Pd dispersion of 1000°C-aged sample is 6.1% and the particle size is 18.4 nm. The calculation results coincide with the TEM results. The results show that after high thermal ageing treatment the Pd particle has a significant growth.

2.4 H_2-TPR

The reducibility of the catalysts was investigated by means of H_2-TPR and the results are displayed in Fig.5. As is well known to us all is that the reduction of PdO species usually occurs at relatively low temperature[27], which is below 200°C as shown in Fig.5. All catalysts exhibit TPR profiles with one main reduction peak which can be assigned to the reduction of PdO to Pd metal. However, the formation of palladium hydrides on the high dispersed Pd is considerably suppressed. It indicates that larger crystallites of metallic Pd appears on the aging catalyst and the dispersed of active PdO decreases during ageing. As shown in Fig.5, the reduction peaks shift to higher temperature and the H_2 consumption values show obvious increase for 1000°C-aged sample. It demonstrates that the amount of active PdO species on the catalyst decreases at high ageing temperature.

2.5 Catalytic performance

Three-way catalytic reactions are of great importance in automobile exhaust purification. In this work, three-way catalysis is carried out using a typical

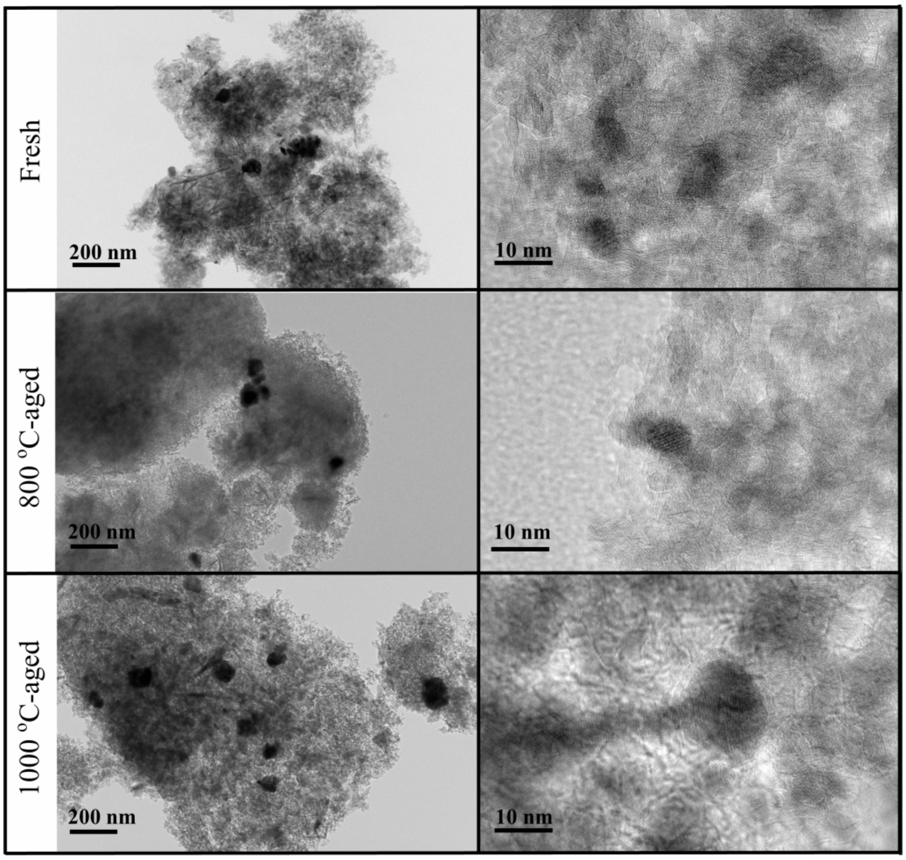

Fig.4 TEM images of different samples 图4 不同催化剂的TEM图像

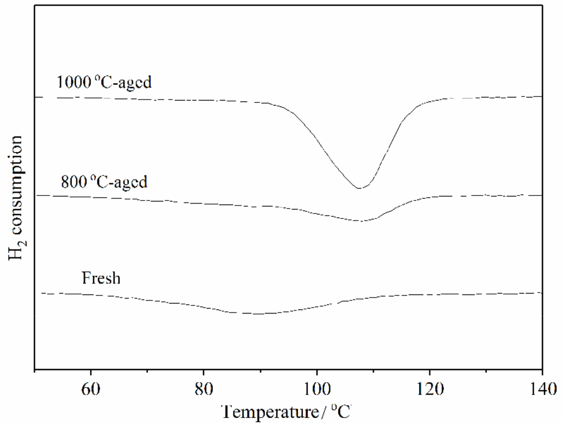

Fig.5 Temperature programmed reduction of various Pd/Al_2O_3 catalysts

图5 不同Pd/Al_2O_3催化剂样品的H_2-TPR图谱

fixed-bed flow reactor in a lean/rich cycling (1.67× 10^{-2} Hz) stream. The typical steady state C_3H_6, NO and CO conversion curves as a function of temperature under the switch of lean and rich feed conditions in three-way catalytic reactions are shown in Fig.6. It can be seen that fresh and 800°C-aged catalysts have almost similar conversion trend of C_3H_6, NO and CO. At low temperature, CO and NO are not converted due to self-inhibition[28]. As the temperature increases from ~200 to 275°C, the CO and NO conversions sharply increase to maximum. The NO and CO conversion rates decrease with further increments in reaction temperature, owing to the fluctuation of O_2 concentration and the partial oxidation by C_3H_6 [15].

$$C_3H_6+4.5O_2\rightarrow 3CO_2+3H_2O \quad (5)$$

$$C_3H_6+3O_2\rightarrow 3CO+3H_2O \quad (6)$$

In contrast, the C_3H_6 conversion reaches a 100% maximum at ≈325°C. However, the great differences are reflected in the 1000°C-aged catalyst. The conversion rates of C_3H_6, NO and CO on 1000°C-aged catalyst peaks at 425°C (100%), 390°C (75%) and 275°C (95%), respectively.

As the three-way catalysis, NO is reduced to N_2, as well as the undesirable secondary products, N_2O and NH_3[5].

$$NO+H_2\rightarrow 0.5N_2+H_2O \quad (7)$$

$$NO+CO \rightarrow 0.5N_2+CO_2 \tag{8}$$

$$NO+2.5H_2 \rightarrow NH_3+H_2O \tag{9}$$

Fig.7 shows the selectivity curves of N_2O and NH_3 formed on the fresh and aged catalysts. It can be seen that the proportion of N_2O and NH_3 is a strong function of the temperature and the ageing temperature. The decreasing N_2O selectivity (Fig.7(a)) is due in part to a declining availability of NO because of the increase of NO desorption rate. That N_2O is the highest at low temperature is a result of the lower rate of N-O bond scission, making NO available to react through N-NO or NO-NO coupling[29].

N_2O formation sharply decreases at higher temperatures due to the increased selectivity to N_2 (Fig.7(c)), a result of an increased rate of N-O bond scission at higher temperatures, minimizing the presence

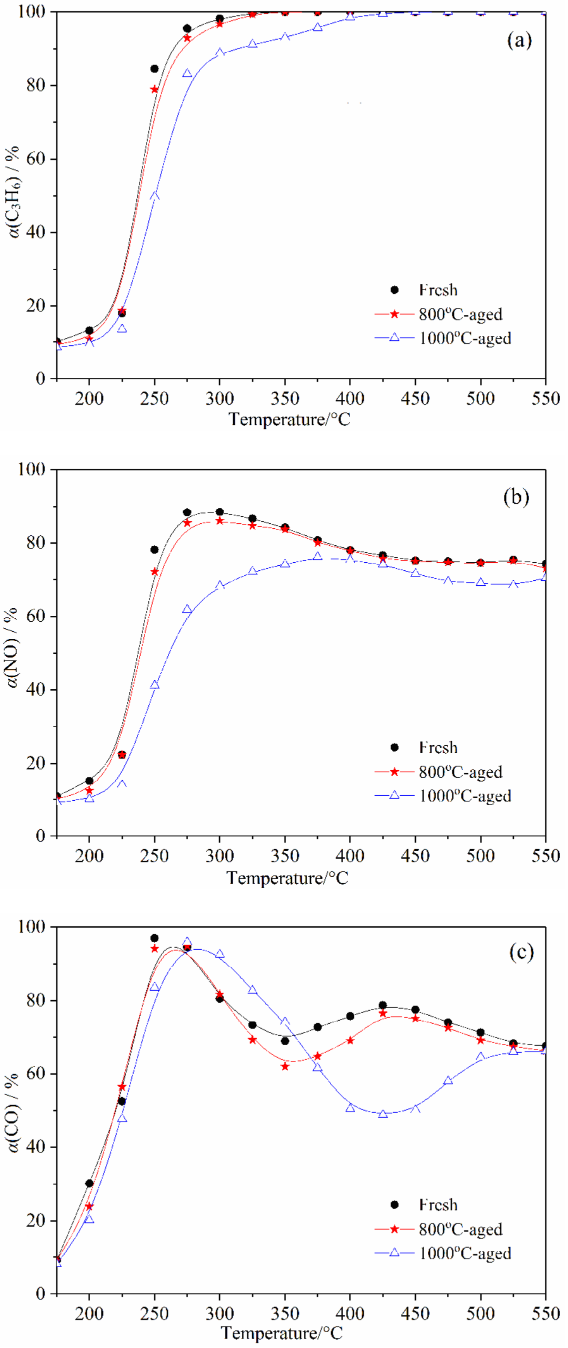

Fig. 6 Conversion curves of (a). C_3H_6, (b). NO and (c). CO of various samples

图 6　不同样品的 C_3H_6 (a)、NO (b)和 CO (c)转化率曲线

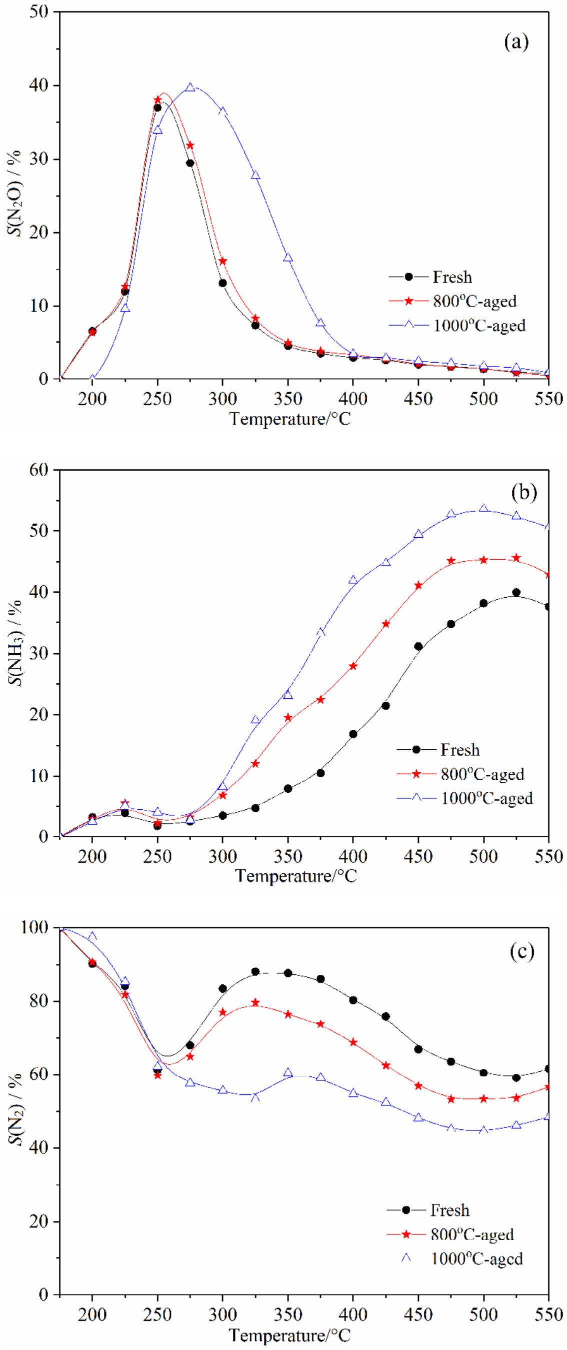

Fig.7 Selectivity curves of (a). N_2O, (b). NH_3 and (c). N_2 of various samples

图 7　不同样品的 N_2O(a)、NH_3(b)和 N_2(c)的选择性曲线

of NO availablility for N-NO coupling, and yielding N-N coupling instead. Other oxidation reactions can occur, including NH_3 oxidation to N_2O and NO:

$$NH_3+O_2\rightarrow 0.5N_2O+1.5H_2O \quad (10)$$

$$NH_3+1.25O_2\rightarrow NO+1.5H_2O \quad (11)$$

In this study, N_2O is mainly detected below 400°C and the selectivity of N_2O rises to ≈38% approximately at 260°C for fresh and 800°C-aged catalysts and then decreases with further reaction temperature increments, whereas the selectivity curve of N_2O formed 1000°C-aged catalyst shows maximum of ≈42% at 275°C and higher selectivity with the increased reaction temperature compared to that of other catalysts. N_2O forms within the same temperature range for cars under standard driving conditions, observing N_2O emissions between 250 and 450ºC [9, 14]. Under lean steady state conditions, the precious metal sites are occupied by an admixture of O, NO and N species. N_2O can form through the reaction[30].

NH_3 starts to form at 200ºC and shows a peaks centered at 225ºC, due to hydroxyl-mediated NH_3 formation[11]. As shown in Fig.6(b), the increasing conversions of CO, NO and C_3H_6 result in a shift to NH_3 as a main N containing product. And NH_3 is main secondary product as the temperature is raised above 300ºC, showing the similar results with literature reported by Mejía-Centeno et al.[5] in this case by reduction of NO by C_3H_6 as well as hydrogen generated from SR and WGS reactions[15].

$$CO+H_2O\rightarrow CO_2+H_2 \quad (12)$$

$$C_3H_6+6H_2O\rightarrow 3CO_2+9H_2 \quad (13)$$

A significant difference in selectivity NH_3 formed on different catalysts starts to be observed above 275ºC, and the NH_3 selectivity increases in following order: fresh catalyst <800ºC-aged catalyst <1000ºC-aged catalyst. Adams et al.[13] found that addition of ceria promotes WGS activity to form more hydrogen, which makes higher amount of NH_3 formed. Nevalainen et al.[12] emphasized that reduced oxygen storage capacity induced by thermal ageing will lead to an increase in amount of formed NH_3, due to the activity loss of NH_3 oxidation.

However, in this case, the increase in the selectivity of NH_3 formed on Pd/Al_2O_3 catalyst caused by thermal ageing is closely related to significant growth of Pd particle. On the basis of the results of XRD, BET, XPS, Raman and Pd dispersion, it demonstrates that the amount of active PdO species on the supported Pd catalyst decreases after calcination at high ageing temperature. NO dissociation (elementary reaction (14)) is thought as the rate-determining step for NO reduction and occurs more readily on larger Pd particle to generate active ·N species (so-called “structure-insensitive reaction”)[31]. As-generated ·N species will react with ·H species to form NH_3, as the following elementary reaction (15).

$$NO\rightarrow \cdot N+\cdot O \quad (14)$$

$$\cdot N+3\cdot H\rightarrow NH_3 \quad (15)$$

3 Conclusions

The study showed that, compared with the fresh catalyst, the Pd particle size of 800°C-aged catalyst grew from 3 nm to 4 nm, and reached 18 nm when it was aged at 1000°C. Raman diagram is also clearly illustrated that the growth of Pd particle size. It also can be obtained from the analysis of the integral area of the optical component, the ratios of Pd^{2+} were 80.8%, 79.4% and 76.5%, respectively. Thus, the number of catalytic active sites decreased. The XRD figure shows that the phase change of γ-Al_2O_3. The transformation leads to the decrease of the BET surface area, which has effect on the catalytic performance of the catalyst. NH_3 as the main toxic by-products, with the increase of aging temperature, the selectivity of NH_3 increased significantly. After aged at 1000°C, the selectivity of NH_3 increased to 53%.

Reference:

[1] WILLIAMSON W B, PERRY J, GANDHI H S, et al. Effects of oil phosphorus on deactivation of monolithic three-way catalysts[J]. Applied catalysis, 1985, 15(2): 277-292.

[2] BRANDENBERGER S, KROCHER O, TISSLER A, et al. The state of the art in selective catalytic reduction of NO_x by ammonia using metala exchanged zeolite catalysts[J]. Catalysis reviews, 2008, 50(4): 492-531.

[3] LAN L, CHEN S, LI H J. et al. Optimized synthesis of highly thermal stable CeO_2-ZrO_2/Al_2O_3 composite for improved Pd-only three-way catalyst[J]. Materal design, 2018, 147: 191-199.

[4] LAN L, LI H, CHEN S, et al. CeO_2-ZrO_2-Al_2O_3 modified by selective doping with SrO for improved Pd-only three-way catalyst[J]. Russia journal of physics chemistry, 2018, 92(4): 696-705.

[5] MEJIA-CENTENO I, CASTILLO S, FUENTES G A. Enhanced emissions of NH_3, N_2O and H_2 from Pd-only TWC and supported model catalysts: Light-off and sulfur level studies[J]. Applied catalysis B: Environmental, 2012(119/120): 234-240.

[6] KEAN A J, BAN-WEISS D L A, HARLEY R A, et al. Trends in on-road vehicle emissions of ammonia[J]. Atmospheric environment, 2009, 43(8): 1565-1570.

[7] ISIDRO MEJIA-CENTENO, ANGEL MARTINES-HERNANDEZ G A. Effect of low-sulfur fuels upon NH_3 and NO emission during operation of commercial three-way catalytic converters[J]. Topics in catalysis, 2007, 43(1/4): 381-385.

[8] SUTTON M A, DRAGOSITS U, TANG Y S, et al. Ammonia emissions from non-agricultural sources in the UK-source testing results[J]. Atmospheric environment, 2000, 34(6): 855-869.

[9] DURBIN T D, WILSON R D, NORBECK J M, et al. Estimates of the emission rates of ammonia from light-duty vehicles using standard chassis dynamometer test cycles[J]. Atmospheric environment, 2002, 36(9): 1475-1482.

[10] HEEB N V, BRIIHLMANN S. Trends of NO, NO_2, and NH_3 emissions from gasoline-fueled Euro-3- to Euro-4-passenger cars[J]. Atmospheric environment, 2008, 42(10): 2543-2554.

[11] WANG C X, XIA W Z, ZHAO Y K. New insight into hydroxyl-mediated NH_3 formation on the Rh-CeO_2 catalyst surface during catalytic reduction of NO by CO[J]. Chinese journal of catalysis, 2017, 38(8): 1399-1405.

[12] NEVALAINEN P, KINNUNEN N M, KIRVESLAHTI A, et al. Formation of NH_3 and N_2O in a modern natural gas three-way catalyst designed for heavy-duty vehicles: The effects of simulated exhaust gas composition and ageing[J]. Applied catalysis A: General, 2017, 552: 30-37.

[13] ADAMS E C, SKOGLUNDH M, CARLSSON P A. Ammonia formation from nitric oxide over Pd-based catalysts in multicomponent feed gas compositions[J]. Catalysis communications, 2017, 95: 26-30.

[14] DURBIN T D, PISANO J T, YOUNGLOVE T, et al. The effect of fuel sulfur on NH_3 and other emissions from 2000-2001 model year vehicles[J]. Atmospheric Environment, 2004, 38(17): 2699-2708.

[15] WANG C X, ZHENG T T, LU J, et al. Three-way catalytic reactions on Rh-based catalyst: Effect of Rh/ceria interfaces[J]. Apply catalysts A: General, 2017, 544: 30-39.

[16] HIETIKKO M, LASSI U, KALLINEN K, et al. Effect of the ageing atmosphere on catalytic activity and textural properties of Pd/Rh exhaust gas catalysts studied by XRD[J]. Applied catalysis A: General, 2004, 277(1): 107-117.

[17] XU W, ZHAN Z, DI L, et al. Enhanced activity for CO oxidation over Pd/Al_2O_3 catalysts prepared by atmospheric-pressure cold plasma[J]. Catalysis today, 2015, 256: 148-152.

[18] HAN Y, GU G, SUN J, et al. Selective hydro-dechlorination of 1,2-dichloroethane to ethylene over Pd-Ag/Al_2O_3 catalysts prepared by surface reduction[J]. Applied surface science, 2015, 355: 183-190.

[19] LIU W W, FENG Y S, WANG G Y, et al. Characterization and reactivity of γ-Al_2O_3 supported Pd-Cu bimetallic nanocatalysts for the selective oxygenization of cyclopentene[J]. Chinese chemical letters, 2016, 27(6): 905-909.

[20] KOLLI T, LASSI U, RAHKAMAA-TOLONEN K, et al. The effect of barium on the catalytic behavior of fresh and aged Pd-Ba-OSC/Al_2O_3 catalysts[J]. Applied catalysis A: General, 2006, 298(1): 65-72.

[21] BRUN M, BERTHET A, BERTOLINI J C. XPS, AES and Auger parameter of Pd and PdO[J]. Journal of electron spectroscopy & related phenomena, 1999, 104(1/3): 55-60.

[22] PEUCKERT M. XPS study on surface and bulk palladium oxide, its thermal stability and a comparison with other noble metal oxides[J]. Cheminform, 1985, 16(39): 2481-2486.

[23] SU S C, CARSTENS J N, BELL A T. A study of the dynamics of Pd oxidation and PdO reduction by H_2 and CH_4[J]. Journal of catalysis, 1998, 176(1): 125-135.

下转第**【53】**页